THE JOURNAL OF NAVIGATION (2017), **70**, 359–378.
doi:10.1017/S037346331600062X

Multi-Feature Maximum Likelihood Association with Space-borne SAR, HFSWR and AIS

Hui Zhang[1], Yongxin Liu[2], Yonggang Ji[3], Linglin Wang[1] and Jie Zhang[3]

[1](*College of Computer Science, Inner Mongolia University, Hohhot 010021, China*)
[2](*College of Electronic Information Engineering, Inner Mongolia University, Hohhot 010021, China*)
[3](*First Institute of Oceanography, State Oceanic Administration, Qingdao 266061, China*)
(E-mail: yxliu@imu.edu.cn)

Ship surveillance is important in maritime management. Space-borne Synthetic Aperture Radar (SAR), High Frequency Surface Wave Radar (HFSWR) and the Automatic Identification System (AIS) are three main sensors for the ship surveillance of large maritime areas. Fusion of these sensors' measurements can produce an accurate ship image distribution in a surveillance area. Data association is fundamental to data fusion. A Maximum Likelihood (ML) association algorithm with multi-feature improvements is proposed to increase detection accuracy and reduce false alarms. The tested features are position, size, heading and velocity. First, the ship measurement model is established. Then, the problem of data association for SAR, HFSWR and AIS is formulated as a multi-dimensional assignment problem. In the data assignment process, Jonker-Volgenant-Castanon (JVC) and Lagrangian relaxation algorithms are applied. Simulation results show that the algorithm proposed here can improve the association accuracy compared with the Nearest Neighbour (NN) and the position-only ML algorithms, using the additional features of length and velocity. Real data experiments illustrate that the algorithm can enhance target identification and reduce false alarms.

KEYWORDS

1. Synthetic Aperture Radar (SAR). 2. High Frequency Surface Wave Radar (HFSWR). 3. Automatic Identification System (AIS). 4. Multi-feature Maximum Likelihood (ML) Association.

Submitted: 10 December 2015. Accepted: 9 August 2016. First published online: 20 October 2016.

1. INTRODUCTION. Ship surveillance is an important area of maritime management, especially for illegal activity detection in the Exclusive Economic Zone (EEZ), such as illegal fishing and smuggling. Many countries have established maritime surveillance systems using various marine sensors (Zhao et al., 2014a).

Synthetic Aperture Radar (SAR), High Frequency Surface Wave Radar (HFSWR) and the Automatic Identification System (AIS) are three main sensors for surveillance of large maritime areas. Both space-borne and air-borne SAR detect ships by comparing the return signal from the ship and the ocean (Pichel et al., 2004). Space-borne SAR has wide coverage and high resolution, and does not have weather restrictions. However, it can only detect ships during satellite transit periods (Ji et al., 2014). Air-borne SAR is usually applied for ship identification or verification during a low-attitude pass (Fingas and Brown, 2001). Due to different Doppler shifts, HFSWR can detect and track ships by discriminating the echoes from ships and the ocean (Ponsford and Wang, 2010). HFSWR has the advantages of continuous surveillance, long range and direct velocity estimation (Grosdidier et al., 2010; Maresca et al., 2014). However, it has a low space resolution (Gurgel et al., 2010). AIS transmits ship information, i.e., position, ship length, ship width, velocity and heading, for ship collision avoidance, but not all ships carry AIS equipment. The ships with installed AIS equipment are usually defined as cooperative ships, while the others are non-cooperative ships (Ji et al., 2014). To sum up, these sensors have their merits and shortcomings in ship surveillance. We cannot obtain an accurate ship traffic image via one sensor alone. Multi-sensor fusion can combine data from different sensors and gain more accurate and specific information than one single sensor (Hall and Llinas, 1997).

Many methods have been exploited in the fusion of space-borne SAR, HFSWR and AIS. The main research is concentrated on the fusion of space-borne SAR and AIS and the fusion of HFSWR and AIS. Within the framework of space-borne SAR and AIS fusion, AIS is usually applied to verify the SAR measurement. Brusch et al. (2011) introduced a ship surveillance algorithm using the TerraSAR-X SAR image, and compared their results with satellite AIS for validation. Zhao et al. (2014a; 2014b) pointed out the lack of systematic theories in SAR and AIS fusion and further proposed an improved association method based on multiple features. This method can be used to identify and track ships. A ship recognition system, including four steps: time matching, position matching, size matching and speed matching, is established using the SAR and AIS data, and this system can identify the ship in nearly real time (Chaturvedi et al., 2012). As for HFSWR and AIS fusion, Dzvonkovskaya et al. (2008) and Dzvonkovskaya and Rohling (2010) adopted a statistical method to analyse the HFSWR detection capacity for various ship types. In their work, the data from HFSWR and AIS was correlated. Recently, we (Zhang et al., 2015) presented a Point Tracks Optimal Algorithm to correlate the data of HFSWR and AIS. The state-of-the-art algorithms for the fusion of radar and AIS data are the measurement-level fusion (Habtemariam et al., 2015) and knowledge-based track fusion (Vivone et al., 2015). On the aspect of the fusion of three sensors, Gurgel et al. (2010) first used AIS and SAR data to verify HF-radar data. Ji et al. (2014) proposed a point association analysis of SAR, HFSWR and AIS to recognise non-cooperative ships under different conditions.

Data association is fundamental to data fusion. The aim of this work is to associate ship measurements from space-borne SAR, HFSWR and AIS, and identify the cooperative ships and suspect non-cooperative ships. Furthermore, the start point of non-cooperative ship tracking can be found from the associated results.

It is known that the simultaneous measurements of space-borne SAR, HFSWR and AIS can only be obtained during the satellite transit period. Space-borne SAR measurements are extracted from SAR images. The measurements mainly contain the

https://doi.org/10.1017/S037346331600062X Published online by Cambridge University Press

position, length, width and heading of ships. HFSWR provides measurements about the ship position (range, and azimuth) and radial velocity. AIS provides the ship position, ship features (including the length, width and ship type), velocity (Speed Over Ground – SOG, Course Over Ground - COG) and heading. It is noted that ship position is the common measurement of three sensors, while ship length, width and heading are the common measurements between space-borne SAR and AIS. Moreover, ship velocity is the common measurement between the HFSWR and AIS.

According to the features of the three sensors, we constructed ship measurement models, and formulated the association of space-borne SAR, HFSWR and AIS as a multi-dimensional assignment problem. In this association problem, the Maximum Likelihood (ML) of the measurements were defined as an association cost. The traditional position-only ML was extended to multi-feature ML, which could improve association accuracy rate.

Based on the models, pair gating technology and an iterative search algorithm were applied to partition the measurements into three types. Different association strategies have been used for different types. The Jonker-Volgenant-Castanon (JVC) algorithm was employed to solve the two-dimensional (2-D) assignment problem (Malkoff, 1997; Jonker and Volgenant, 1987), and Lagrangian relaxation algorithm was used to work out the 3-D association problem. The three-dimensional (3-D) assignment problem belongs to the Non-deterministic Polynomial-time hard (NP hard) problem generally solved by heuristic and relaxation algorithms. The Lagrangian relaxation approach was proved suitable in solving the NP hard problem in performance and real-time application (Deb et al., 1997).

The organisation of this paper is as follows. Section 2 introduces the ship measurement models. The association problem is formulated as an assignment problem in Section 3. The data association procedure is presented in Section 4. Section 5 gives both the experiment results of the simulation data and the real detected data. Conclusions are given in Section 6.

2. SHIP MEASUREMENT MODEL.

SAR position and AIS position are measured in the World Geodetic System 84 (WGS84), while HFSWR position is measured in the radar polar coordinates system. For convenience, the measurement model is constructed in Cartesian coordinates.

2.1. *Ship Measurement Model.*

The ship state vector at time k is defined as

$$\boldsymbol{X}(k) = ([\, x(k) \quad \dot{x}(k) \quad y(k) \quad \dot{y}(k) \,])^T \tag{1}$$

where $x(k)$, $y(k)$ and $\dot{x}(k)$, $\dot{y}(k)$ are the position and velocity components in x, y directions. $(\cdot)^T$ is the transpose function (Maresca et al., 2014). The ship measurement model is defined as

$$\boldsymbol{z}(k) = h(\boldsymbol{X}(k)) + w(k) \tag{2}$$

where $\boldsymbol{z}(k)$ is the measurement vector, $h(\boldsymbol{X}(k))$ is the measurement function and $w(k)$ is the measurement noise (Habtemariam et al., 2015; Li and Jilkov, 2003).

2.2. *SAR Measurement Model.*

Space-borne SAR only provides measurements at the satellite transit time T_{tran}. Therefore, the measurement model of SAR is

https://doi.org/10.1017/S037346331600062X Published online by Cambridge University Press

defined as

$$\boldsymbol{z}_s(\mathrm{k}) = \begin{cases} h_s(\boldsymbol{X}(k)) + w_s(k) & k = T_{tran} \\ 0 & otherwise \end{cases} \tag{3}$$

where $h_s(\boldsymbol{X}(k)) = [\, x(k) \quad y(k) \quad l(k) \quad w(k) \quad h(k) \,]^T$ is the measurement function of SAR. $l(k)$ is ship length, $w(k)$ is ship width, and $h(k)$ is ship heading. $w_s(k)$ is the SAR measurement noise. The measurement noise is assumed to be zero-mean white Gaussian, and the covariance $\boldsymbol{R}_s$ is defined as

$$\boldsymbol{R}_s = \begin{bmatrix} \sigma_x^2 & 0 & 0 & 0 & 0 \\ 0 & \sigma_y^2 & 0 & 0 & 0 \\ 0 & 0 & \sigma_l^2 & 0 & 0 \\ 0 & 0 & 0 & \sigma_w^2 & 0 \\ 0 & 0 & 0 & 0 & \sigma_h^2 \end{bmatrix} \tag{4}$$

where σ is the standard deviation.

2.3. *HFSWR Measurement Model.* HFSWR detects the ship target in continuous-time and the HFSWR measurement model is given by

$$\boldsymbol{z}_h(\mathrm{k}) = h_h(\boldsymbol{X}(k)) + w_h(k) \tag{5}$$

where $h_h(\boldsymbol{X}(k)) = [\, r(k) \quad \theta(k) \quad v_r(k) \,]^T$ is the measurement function of HFSWR. $r(k)$ is the range, $\theta(k)$ is the azimuth, and $\mathrm{v}_r(k)$ is the radial velocity. The measurement equations are listed as follows.

$$\begin{aligned} r(\mathrm{k}) &= \sqrt{(x(k) - x_s)^2 + (y(k) - y_s)^2} \\ \theta(k) &= \tan^{-1}\left(\frac{y_s - y(k)}{x_s - x(k)}\right) \\ v_r(k) &= \frac{(x(k) - x_s)\dot{x}(k) + (y(k) - y_s)\dot{y}(k)}{\sqrt{(x(k) - x_s)^2 + (y(k) - y_s)^2}} \end{aligned} \tag{6}$$

where x_s and y_s describe the position of the radar stations. $w_h(k)$ is the HFSWR measurement noise, which is assumed to be zero-mean white Gaussian. The covariance $\boldsymbol{R}_h$ is defined as

$$\boldsymbol{R}_h = \begin{bmatrix} \sigma_r^2 & 0 & 0 \\ 0 & \sigma_\theta^2 & 0 \\ 0 & 0 & \sigma_{v_r}^2 \end{bmatrix} \tag{7}$$

2.4. *AIS Measurement Model.* The time interval for AIS measurements reporting depends on the types of AIS equipment and ship's dynamic state (Xiao et al., 2015; Habtemariam et al., 2015). So the AIS measurement model is defined as

$$\boldsymbol{z}_a(k) = \begin{cases} h_a(\boldsymbol{X}(k)) + w_a(k) & k = t_{report}^m \\ DR(\boldsymbol{X}(\mathrm{k})) & t_{report}^m < k < t_{report}^{m+1} \end{cases} \tag{8}$$

where $h_a(\boldsymbol{X}(k)) = [\, x(k) \quad y(k) \quad v_{sog}(k) \quad \theta_{cog}(k) \,]^T$ is the measurement function of AIS and $DR(\boldsymbol{X}(k))$ is a Dead Reckoning (DR) function. $v_{sog}(k)$ is the speed over

https://doi.org/10.1017/S037346331600062X Published online by Cambridge University Press

ground, and $\theta_{cog}(k)$ is course over ground. If the sampling time k equals the mth AIS report time t^m_{report}, the AIS measurements are directly provided by the AIS reports. If not, the DR method is employed to predict the AIS position and velocity by the AIS reports (Chaturvedi et al., 2012). Herein, it is assumed that there are no false alarms and missed detections of the AIS measurements and the measurement noise $w_a(k)$ is zero.

3. PROBLEM FORMULATION.

Based on the measurement models established in Section 2, we formulated the association problem as an N-Dimensional (N-D) assignment problem. We extended the previous work of Pattipati et al. (1992) and Deb et al. (1997) to the maritime surveillance scenario.

The association is under the assumptions:

- The SAR and HFSWR measurements may contain missed detections and false alarms, while the AIS measurements have no missed detections and false alarms.
- The cooperative ships should provide ship information to AIS.
- The non-cooperative ships should be detected by both SAR and HFSWR, but do not provide information to AIS.
- Ships which did not provide the information to AIS and are detected by only one of either SAR and HFSWR sensors, cannot be recognised as non-cooperative ships.

Considering the missed detections in association, we define a dummy measurement in each sensor. $\boldsymbol{z}_{s0}(\mathrm{k})$ and $\boldsymbol{z}_{h0}(\mathrm{k})$ represents the missed detection caused by SAR and HFSWR, while $\boldsymbol{z}_{a0}(\mathrm{k})$ represents the missed detection caused by non-cooperative ships in AIS.

A complete set $\boldsymbol{Z}(\mathrm{k})$, i.e., the union of all three measurements at time k, is defined as

$$\boldsymbol{Z}(k) = \{\boldsymbol{z}_{si_s}(\mathrm{k})\}_{i_s=0}^{n_s} \cup \{\boldsymbol{z}_{hi_h}(k)\}_{i_h=0}^{n_h} \cup \{\boldsymbol{z}_{ai_a}(k)\}_{i_a=0}^{n_a} \tag{9}$$

n_s, n_h, and n_a are the numbers of SAR, HFSWR and AIS measurements, respectively. i_s, i_h and i_a are the detection indices of each measurement. Since time k is a constant value in the association of space-borne SAR, HFSWR and AIS, k is omitted below.

The union set of all feasible partitions is defined as $\zeta = \{\gamma_0, \gamma_1, \gamma_2, \cdots, \gamma_\alpha\}$. $\gamma_{\mathrm{i}}(i \neq 0)$ is one of the feasible partitions and $\gamma_0 = \{\boldsymbol{Z} = \phi\}$ represents where the measurements of SAR and HFSWR are all false alarms.

Based on the definitions above, the association problem can be described as a problem of solving the maximum probability defined as

$$\max_{\gamma_1\gamma_2\cdots\gamma_\alpha} \{p(\Gamma = \gamma|\boldsymbol{Z})|\gamma \in \zeta\} \tag{10}$$

where $p(\cdot)$ is the probability of partitions γ and Γ is the event. Our goal is to choose the partition γ to find the most probable event. Here, the ML ratio $\max_{\gamma\in\zeta} \dfrac{L(\gamma)}{L(\gamma_0)}$ is used to replace p in Equation (10). $L(\gamma)$ is the ML of partition γ. The traditional ML only about the target position is defined as

$$L(\gamma) = p[\boldsymbol{Z}|\gamma] = \left[\prod_{\boldsymbol{Z}_{i_s i_h i_a}\in\gamma} \Lambda(\boldsymbol{Z}_{i_s i_h i_a}|(x,y))\right] \cdot (P_{Fh})^{n_h - T_h(\gamma)} \cdot (P_{Fs})^{n_s - T_s(\gamma)} \tag{11}$$

https://doi.org/10.1017/S037346331600062X Published online by Cambridge University Press

where $\Lambda(\boldsymbol{Z}_{i_s i_h i_a}|(x,y))$ is the likelihood that the measurements $\boldsymbol{Z}_{i_s i_h i_a}$ originate from the target in (x, y) position. P_{Fs} and P_{Fh} are the false alarm probabilities of SAR and HFSWR, respectively. $T_s(\gamma)$ and $T_h(\gamma)$ are the numbers of targets in SAR and HFSWR measurements, respectively. Because of the poor position resolution of HFSWR measurements, the association based only on the position may lead to the wrong association. Alternatively, multi-feature ML is used to improve the association accuracy rate. This is defined as

$$L(\gamma) = p[\boldsymbol{Z}|\gamma] = \left[\prod_{\boldsymbol{Z}_{i_s i_h i_a} \in \gamma} \Lambda(\boldsymbol{Z}_{i_s i_h i_a}|v_1, v_2, \cdots, v_m)\right] \cdot (P_{Fh})^{n_h - T_h(\gamma)} \cdot (P_{Fs})^{n_s - T_s(\gamma)} \tag{12}$$

where $v_1, v_2, \cdots v_m$ are the different features of target. $\Lambda(\boldsymbol{Z}_{i_s i_h i_a}|v_1, v_2, \cdots, v_m)$ represents the probability of measurement $\boldsymbol{Z}_{i_s i_h i_a}$ which originates from the target with the feature vector $v_1, v_2, \cdots v_m$.

Since the features vector of a target is unknown in the association, the $v_1, v_2, \cdots v_m$ is replaced by the estimate value given by

$$\hat{L}(\gamma) = p[\boldsymbol{Z}|\gamma] = \left[\prod_{\boldsymbol{Z}_{i_s i_h i_a} \in \gamma} \hat{\Lambda}(\boldsymbol{Z}_{i_s i_h i_a}|\hat{v}_1, \hat{v}_2, \cdots, \hat{v}_m)\right] \cdot (P_{Fh})^{n_h - T_h(\gamma)} \cdot (P_{Fs})^{n_s - T_s(\gamma)} \tag{13}$$

where $\hat{L}(\gamma)$ is the estimated value of $L(\gamma)$. For cooperative ships, AIS information is treated as the estimated value. For non-cooperative ships, SAR position information is treated as the estimated value. The range and azimuth of AIS measurements are converted from the position (x, y) by Equation (6). The radial velocity is converted from course over ground θ_{cog} and speed over ground v_{sog} by

$$v_r = -v_{sog} \times cos(\theta - \theta_{cog}) \tag{14}$$

v_r is a positive number when the ship sails towards the radar station, and v_r is a negative number when the ship sails away from the station.

According to the features of the three sensors, different features are used in the association of different sensor pairs. The ship position, length, width and heading can be selected as the feature vector for SAR and AIS ML. The ship position and radial velocity can be selected as the feature vector for HFSWR and AIS. Only the position feature can be selected for SAR and HFSWR. Table 1 shows the details. For the association with HFSWR, position of (range, azimuth) is more suitable than position of (x, y) because the HFSWR measurement error of position (x, y) increases with an increase in range.

Here, we assumed that all the feature measurements are normally distributed with the standard deviation σ, and are independent. Therefore, $\hat{L}(\gamma)$ is given by

$$\begin{aligned}\hat{L}(\gamma) = &\left[P_{Ds} \cdot N\left(\hat{x}, \sigma_x^2\right) \cdot N\left(\hat{y}, \sigma_y^2\right) \cdot N\left(\hat{l}, \sigma_l^2\right) \cdot N\left(\hat{w}, \sigma_w^2\right) \cdot N\left(\hat{h}, \sigma_h^2\right)\right]^{1-\delta_{0i_s}} \cdot [1 - P_{Ds}]^{\delta_{0i_s}} \\ &\cdot (P_{Fs})^{n_s - T_s(\gamma)} \cdot \left[P_{Dh} \cdot N\left(\hat{r}, \sigma_r^2\right) \cdot N\left(\hat{\theta}, \sigma_\theta^2\right) \cdot N\left(\hat{v}_r, \sigma_{v_r}^2\right)\right]^{1-\delta_{0i_h}} \cdot [1 - P_{Dh}]^{\delta_{0i_h}} \cdot (P_{Fh})^{n_h - T_h(\gamma)}\end{aligned} \tag{15}$$

where P_{Ds} and P_{Dh} are the detection probabilities of SAR and HFSWR, respectively.

https://doi.org/10.1017/S037346331600062X Published online by Cambridge University Press

Table 1. The features used in the association of different sensor pair.

Sensor pair	SAR & AIS	HFSWR & AIS	SAR & HFSWR
The features used in the association	Position (x, y) Ship length Ship width Ship heading	Position (range, azimuth) Radial velocity	Position (range, azimuth)

$N(\mu,\sigma^2)=\frac{1}{\sqrt{2\pi}\sigma}e^{-\frac{(z-\mu)^2}{2\sigma}}$ is given by

$$N(\mu,\sigma^2)=\frac{1}{\sqrt{2\pi}\sigma}e^{-\frac{(z-\mu)^2}{2\sigma}} \tag{16}$$

if taking into account the missed detections in the association, the indicator δ_{0i} is given as

$$\delta_{0i}=\begin{cases}1 & if\quad a\quad target\quad is\quad missed\quad by\quad sensor\\ 0 & otherwise\end{cases} \tag{17}$$

$L(\gamma_0)$ is given by

$$L(\gamma_0)=p[\boldsymbol{Z}|\gamma_0]=(P_{Fh})^{n_h}\cdot(P_{Fs})^{n_s} \tag{18}$$

let $\min_{\gamma\in\zeta}\frac{L(\gamma_0)}{\hat{L}(\gamma)}$ replace $\max_{\gamma\in\zeta}\frac{\hat{L}(\gamma)}{L(\gamma_0)}$, the maximum problem becomes a minimum one

$$J^*=\min_{\gamma\in\zeta}J(\gamma)=\min_{\gamma\in\zeta}[\ln L(\gamma_0)-\ln\hat{L}(\gamma)] \tag{19}$$

then, the association problem can be formulated as a multi-assignment one

$$J(\rho)=\sum_{i_s=0}^{n_s}\sum_{i_h=0}^{n_h}\sum_{i_a=0}^{n_a}c_{i_si_hi_a}\rho_{i_si_hi_a} \tag{20}$$

subject to

$$\begin{aligned}&\sum_{i_h=0}^{n_h}\sum_{i_s=0}^{n_s}\rho_{i_si_hi_a}=1 \qquad i_a=1,2,\ \cdots,n_a\\ &\sum_{i_a=0}^{n_a}\sum_{i_h=0}^{n_h}\rho_{i_si_hi_a}=1 \qquad i_s=1,2,\ \cdots,n_s\\ &\sum_{i_s=0}^{n_s}\sum_{i_a=0}^{n_a}\rho_{i_si_hi_a}=1 \qquad i_h=1,2,\ \cdots,n_h\end{aligned} \tag{21}$$

in which the defined two-valued variables $\rho_{i_si_hi_a}$ are given by

$$\rho_{i_si_hi_a}=\begin{cases}1 & if\quad \boldsymbol{Z}_{i_si_hi_a}\in\gamma\\ 0 & otherwise\end{cases} \tag{22}$$

https://doi.org/10.1017/S037346331600062X Published online by Cambridge University Press

and the association cost $c_{i_s i_h i_a}$ is defined by

$$\begin{aligned} c_{i_s i_h i_a} &= \ln L(\gamma_0) - \ln \hat{L}(\gamma) \\ &= (1-\delta_{0i_s})\left(\ln\left(P_{Ds}\cdot N\left(\hat{x},\sigma_x^2\right)\cdot N\left(\hat{y},\sigma_y^2\right)\cdot N\left(\hat{l},\sigma_l^2\right)\cdot N\left(\hat{w},\sigma_w^2\right)\cdot N\left(\hat{h},\sigma_h^2\right)\right)\right) \\ &\quad - \delta_{0i_s}\ln(1-P_{Ds}) \\ &\quad + (1-\delta_{0i_h})\left(\ln\left(P_{Dh}\cdot N\left(\hat{r},\sigma_r^2\right)\cdot N\left(\hat{\theta},\sigma_\theta^2\right)\cdot N\left(\hat{v},\sigma_v^2\right)\right)\right) - \delta_{0i_h}\ln(1-P_{Dh}) \\ &\quad + T_h(\gamma)(\ln P_{Fh}) + T_s(\gamma)(\ln P_{Fs}) \end{aligned} \tag{23}$$

since the number and probability of false alarms are constant, $c_{i_s i_h i_a}$ is not affected by the two latter terms. It can be simplified as

$$\begin{aligned} c_{i_s i_h i_a} &= \ln L(\gamma_0) - \ln \hat{L}(\gamma) \\ &= (1-\delta_{0i_s})\left(\ln\left(P_{Ds}\cdot N\left(\hat{x},\sigma_x^2\right)\cdot N\left(\hat{y},\sigma_y^2\right)\cdot N\left(\hat{l},\sigma_l^2\right)\cdot N\left(\hat{w},\sigma_w^2\right)\cdot N\left(\hat{h},\sigma_h^2\right)\right)\right) \\ &\quad - \delta_{0i_s}\ln(1-P_{Ds}) \\ &\quad + (1-\delta_{0i_h})\left(\ln\left(P_{Dh}\cdot N\left(\hat{r},\sigma_r^2\right)\cdot N\left(\hat{\theta},\sigma_\theta^2\right)\cdot N\left(\hat{v},\sigma_v^2\right)\right)\right) - \delta_{0i_h}\ln(1-P_{Dh}) \end{aligned} \tag{24}$$

4. DATA ASSOCIATION FOR SAR, HFSWR AND AIS.

The data association procedure contains two phases: measurement partition and data association.

4.1. *Measurement Partition.*

In order to apply the multi-assignment algorithm, the complete set $\boldsymbol{Z}$ is firstly divided into many different combinations. These combinations contain all the possible associated measurements. The pair gating method is used to find the feasible associated target measurements between each pair of sensors. Furthermore, an iterative search method is employed to ensure that the divided combination covers all the possible associated target measurements.

4.1.1. *Pair Gating.*

Different sensor pairs have different gating thresholds. The three gating thresholds are defined as follows.

- The gating threshold between AIS and SAR measurements is given by

$$\mathrm{D}(i_a, i_s) = \sqrt{|\boldsymbol{z}_{ai_a}(x) - \boldsymbol{z}_{si_s}(x)|^2 + |\boldsymbol{z}_{ai_a}(y) - \boldsymbol{z}_{si_s}(y)|^2} \le D_{\max} \tag{25}$$

  where $\mathrm{D}(i_a, i_s)$ denotes the Euclidean distance between the i_ath AIS and i_sth SAR measurement. $D_{\max}$ is the Euclidean distance threshold between the SAR and AIS measurement. It is related to the target space positioning accuracy of SAR. The space positioning accuracy is affected mainly by geometric positioning accuracy and resolution of SAR. $D_{\max}$ is also influenced by the azimuth displacement, which is caused by the Doppler shift of a fast moving target (Tunaley, 2003). Here, based on SAR resolution and the experiment's statistical data, $D_{\max}$ selected here is 2 km.

https://doi.org/10.1017/S037346331600062X Published online by Cambridge University Press

- The gating threshold between AIS and HFSWR measurements is given by

$$\begin{aligned} |\boldsymbol{z}_{hi_h}(r) - \boldsymbol{z}_{ai_a}(r)| &\le r_{\max} \\ |\boldsymbol{z}_{hi_h}(\theta) - \boldsymbol{z}_{ai_a}(\theta)| &\le \theta_{\max} \\ |\boldsymbol{z}_{hi_h}(v_r) - \boldsymbol{z}_{ai_a}(v_r)| &\le V_{\max} \end{aligned} \tag{26}$$

  The range, azimuth and radial velocity of AIS measurement can be computed by Equations (6) and (14). $r_{\max}$, $\theta_{\max}$ and $V_{\max}$ are the range, azimuth and radial velocity gating threshold of the HFSWR and AIS. These three gating thresholds can refer to the accuracy of the HFSWR detection, and the accuracy is related to the HFSWR resolution. HFSWR range resolution is determined by the signal bandwidth, azimuth resolution is related to the antenna aperture and radial velocity resolution is related to the radar coherent integration time. The value of $r_{\max}$ selected here is 2 km, $\theta_{\max}$ selected here is 5°, and $V_{\max}$ selected here is 2 km/h.
- The gating threshold between SAR and HFSWR measurements is given by

$$\begin{aligned} |\boldsymbol{z}_{hi_h}(r) - \boldsymbol{z}_{si_s}(r)| &\le r_{\max} \\ |\boldsymbol{z}_{hi_h}(\theta) - \boldsymbol{z}_{si_s}(\theta)| &\le \theta_{\max} \end{aligned} \tag{27}$$

since the measurement error of HFSWR is greater than the error of SAR, $r_{\max}$ and $\theta_{\max}$ are also selected as the gating threshold between the SAR and HFSWR. The range and azimuth value of SAR are converted by Equation (6).

4.1.2 *Iterative Search.* The iterative search method can select all the possible associated target measurements and put them into one combination. Thus, all data can be divided into several combinations. The method can begin with any measurement of any sensor. Here, we use the i_ath AIS measurement as the start point to demonstrate the iterative search method. The main steps are as follows:

- Step 1: *AIS* set, only one measurement $\boldsymbol{z}_{ai_a}$, is defined. Furthermore, two empty sets, *SAR* and *HFSWR* set, are defined.
- Step 2: Record the elements number of *AIS, SAR* and *HFSWR* set.
- Step 3: Use every measurement in *AIS* set, traverse all the SAR measurements, find all the SAR measurements that meet the gating threshold in Equation (25) with AIS measurements, and add them into *SAR* set; Also, *HFSWR* set is added with the same step.
- Step 4: Use every measurement in *SAR* set, traverse all the HFSWR measurements, find all the HFSWR measurements meeting the gating threshold in Equation (27) with *SAR* measurements, and add them into *HFSWR* set; Also, *AIS* set is added with the same step.
- Step 5: Use every measurement in *HFSWR* set, traverse all the AIS measurements, find all the AIS measurements that meet the gating threshold in Equation (26) with HFSWR measurements, and add them into *HFSWR* set; Also, *SAR* set is added with the same step.
- Step 6: if the present elements number of *AIS, SAR* and *HFSWR* set are all equal to the elements number in Step 2, go to Step 7; else, go to Step 2 for iteration.
- Step 7: The union of *AIS, SAR* and *HFSWR* set are the iterative search results.

https://doi.org/10.1017/S037346331600062X Published online by Cambridge University Press

After the iterative search, we can divide all the measurements into different combinations. These combinations have three types:

- Type 1: The union of *AIS, SAR* and *HFSWR* set has measurements of one sensor.
- Type 2: The union of *AIS, SAR* and *HFSWR* set has measurements of two sensors. These measurements may originate from the non-cooperative ships or the cooperative ships with missed detections.
- Type 3: The union of *AIS, SAR* and *HFSWR* set has measurements of three sensors. These measurements may originate from the cooperative ships.

4.2. *Data Association.* As for the divided combinations, different association algorithms are applied. For the combinations of Type 1, the SAR and HFSWR measurements are generally regarded as false alarms and the AIS measurements are regarded as the cooperative ships. For the combinations of Type 2, the association problem is a 2-D assignment problem and can be solved by the JVC algorithm. For the combinations of Type 3, the association problem is a 3-D assignment problem and can be solved by a Lagrangian relaxation algorithm.

4.2.1. *JVC Algorithms.* For the traditional 2-D assignment problem, JVC algorithms can provide an optimal solution in polynomial time (Kadar et al., 1997). When the combinations have measurements of two sensors, the 2-D assignment algorithm is formulated as follows.

$$J(\rho) = \min \sum_{i=0}^{n_i} \sum_{j=0}^{n_j} c_{ij}\rho_{ij} \tag{28}$$

subject to

$$\begin{aligned} \sum_{j=0}^{n_j} \rho_{ij} &= 1 \qquad i = 1, 2, \cdots, n_i \\ \sum_{i=0}^{n_i} \rho_{ij} &= 1 \qquad j = 1, 2, \cdots, n_j \end{aligned} \tag{29}$$

The value of c_{ij} can be obtained from Equation (24). The optimal solution is to find the point to point assignment so that the sum of c_{ij} is the minimum value. We applied the JVC algorithm to solve the HFSWR and AIS association problem in our previous work (Zhang et al., 2015). Its results showed that the JVC algorithm is feasible for the 2-D assignment problem in both performance and real time.

4.2.2. *Lagrangian Relaxation Algorithm.* A Lagrangian relaxation algorithm is a suboptimal solution of the 3-D assignment, which can provide the upper and lower bounds of the assignment problem (Poore and Robertson III, 1997). The lower bound can be usually obtained by the relaxed 2-D assignment solutions. The upper bound can be obtained by the feasible solutions of 3-D assignment (Deb et al., 1997).

The main steps of the Lagrangian relaxation algorithm are as follows:

- Initial Step: Initialise the value of variables.
- Lagrangian multiplier $u_{ai_a} = 0$, iterate time $iter = 0$, maximum iterate times $maxiter = 200$, upper bound $f_{upper} = \infty$, and lower bound $f_{\text{lower}} = -\infty$. The *gap*

https://doi.org/10.1017/S037346331600062X Published online by Cambridge University Press

is defined as Equation (30), and minimum gap threshold $mingap = 0$.

$$gap = \left(f_{upper} - f_{lower}\right)/|f_{lower}| \tag{30}$$

- Iteration Step: firstly, the reduced costs are computed as

$$d^2_{i_s i_h} = \min_{i_a}(c_{i_s i_h i_a} - u_{ai_a}) \tag{31}$$

Secondly, the 3-D assignment is relaxed as a 2-D assignment problem with $d^2_{i_s i_h}$ and a new two-valued variable $w_{i_s i_h}$ is given by

$$J2(\rho) = \min \sum_{i_s=0}^{n_s} \sum_{i_h=0}^{n_h} w_{i_s i_h} d^2_{i_s i_h} + \sum_{i_a}^{n_a} u_{ai_a} \tag{32}$$

subject to

$$\begin{aligned} \sum_{i_s=0}^{n_s} w_{i_s i_h} &= 1 \qquad i_h = 1, 2, \cdots, n_h \\ \sum_{i_h=0}^{n_h} w_{i_s i_h} &= 1 \qquad i_s = 1, 2, \cdots, n_s \end{aligned} \tag{33}$$

This 2-D problem is solved by a JVC algorithm. Then, based on the results of the 2-D problem, the 3-D problem is solved as another 2-D problem as

$$J3(\rho) = \min \sum_{i_r=0}^{n_r} \sum_{i_h=0}^{n_h} w_{i_r i_a} d^3_{i_s i_h i_a} \tag{34}$$

Subject to

$$\begin{aligned} \sum_{i_r=0}^{n_r} w_{i_r i_a} &= 1 \qquad i_a = 1, 2, \cdots, n_a \\ \sum_{i_a=0}^{n_a} w_{i_r i_a} &= 1 \qquad i_r = 1, 2, \cdots, n_r \end{aligned} \tag{35}$$

where i_r are the 2-D assignment results of Equation (32), which are the index of assignment results for SAR and HFSWR. n_r is the number of 2-D assignment results. The value of $d^3_{i_s i_h i_a}$ equals $c_{i_s i_h i_a}$. Finally, Lagrangian Multiplier u_{ai_a} is updated with the new price update algorithm (Pattipati et al., 1992).

- Results output Step: Update the value of *gap* as Equation (30), and update the value of f_{upper}, f_{lower} and *iter* by

$$\begin{aligned} f_{\text{lower}} &= \max(f_{lower}, J2) \\ f_{upper} &= \min\left(f_{upper}, J3\right) \\ iter &= iter + 1 \end{aligned} \tag{36}$$

https://doi.org/10.1017/S037346331600062X Published online by Cambridge University Press

If the iteration meets the terminate condition ($gap < mingap$) or ($iter > maxiter$), association results are output. Otherwise, the iteration step is continued.

5. EXPERIMENT RESULTS. In this section, the evaluation metric is first presented for association of SAR, HFSWR, and AIS. Then, the proposed method is verified by simulated and real data.

5.1. *Evaluation Metric.* Since the errors of SAR and HFSWR are different orders of magnitude, different metrics are used to evaluate the association performance. The evaluation metrics are defined as follows:

- Mean position error: mean position error between SAR and AIS is defined as

$$\bar{\varepsilon}_{\text{pos}} = \frac{1}{num\_s} \sum_{num=1}^{num\_s} \sqrt{(\hat{x} - \boldsymbol{z}_{si_s}(x))^2 + (\hat{y} - \boldsymbol{z}_{si_s}(y))^2} \tag{37}$$

- where num_s is the number of SAR and AIS association results. $\hat{x}$, $\hat{y}$ are the estimated value.
- Mean range error, mean azimuth error, mean radial Velocity error: the mean error between HFSWR and AIS or SAR is defined as

$$\bar{\varepsilon} = \frac{1}{num\_h} \sum_{num=1}^{num\_h} |\hat{\boldsymbol{z}} - \boldsymbol{z}_{hi_h}| \tag{38}$$

- where the num_h is the number of HFSWR and AIS or SAR association results. $\hat{\boldsymbol{z}}$ is the estimated value.
- Accuracy rate. The association accuracy rate is defined for the evaluation of the simulated data, which is given by

$$acc\_rate = \frac{num\_right}{num\_associate} \tag{39}$$

where *num_right* is the number of correctly associated measurements, and *num_associate* is the number of associated results.

5.2. *Simulated Data Association.* The simulated data contains cooperative ships, non-cooperative ships and false alarms.

5.2.1. *Simulated Data Parameters.* The cooperative ships data is simulated based on AIS measurements in a real ship detection scenario. These measurements are extracted from a Terrestrial AIS report from 06:47 to 06:57 on November 13, 2013. The Dead Reckoning (DR) method is employed to predict the AIS position and velocity at 06:52. The SAR and HFSWR measurements of cooperative ships are simulated with the AIS data plus the measurement noise $w_s(k)$ and $w_h(k)$, with the detect probability P_{Ds} and P_{Dh}. For non-cooperative ships, the simulated data are uniformly distributed in the measurement area. These measurements are detected by SAR and HFSWR with the detection probability P_{Ds} and P_{Dh}, and not detected by AIS. False alarms are simulated with only SAR or HFSWR measurements, and the false alarm probability is P_{Fs} and P_{Fh}, respectively.

Different resolutions SAR and HFSWR measurements are simulated in this section. Three resolution SAR images are usually used in ship detection: high resolution (pixel

https://doi.org/10.1017/S037346331600062X Published online by Cambridge University Press

resolution less than 3 m), medium resolution (pixel resolution about 8 to 10 m) and low resolution SAR images (pixel resolution about 25 m). Due to the limitations of the resolution, it is hard to identify the exact ship length and width from the low resolution SAR images. Thus, only high and medium resolution SAR scenarios are simulated. The maximum errors of ship length and width extracted from the SAR images are about three pixels of image compared with the real ship. In medium resolution SAR images, the ship heading is estimated through the Radon transform (Margarit and Tabasco, 2011), the maximum heading error is about 15°. In high resolution SAR images, the maximum heading error is about 7·5°. For the HFSWR simulation, the Wellen Radar (WERA) has high resolution on ship detection. Referring to Maresca et al. (2014), the simulation data on WERA is selected as the parameters set for high resolution HFSWR, and our HFSWR parameters are selected as the parameters set for low resolution.

Table 2 highlights the main parameters of our simulated scenarios, in which the value of standard deviations σ are one-third of the maximum errors, and detection and false alarm probabilities are derived from the experimental statistics.

5.2.2. *Monte Carlo simulations.* The influence of different features and parameters is evaluated by 10^2 Monte Carlo (MC) simulations. From the simulation results, we draw conclusions as follows:

- Association with ship length and radial velocity features can improve the association accuracy rate. Its association accuracy rate is always higher than the ML association without those features.
- Association with ship heading and azimuth features cannot improve the association rate. Association accuracy rate is always lower than the ML association without those features.
- Association with ship width feature can improve the association accuracy rate when $\sigma_w \geq 6$ m. This means that association with the ship width feature can improve the association accuracy rate only in high resolution SAR.

Real data association, considered in this paper, is the association of medium resolution SAR and low resolution HFSWR. The simulated results of this scenario are analysed as follows. The maximum standard deviations of Table 2 are selected as the simulated parameters. Table 3 shows the results of the different features combination with the multi-feature ML association algorithm. The accuracy rate of multi-feature with position, ship length, range and radial velocity is the highest. Table 4 compares three association algorithms. Multi-feature ML association brings the 12·4% percentage points improvement of the association accuracy rate, compared with the traditional position-only ML association. Figure 1 shows the association accuracy rate of three association algorithms in 10^2 MC simulations.

5.3. *Real Data Association.* Experiments are conducted on a real ship detection scenario on 13 November 2013. The association experiments are based on data from space-borne SAR, coastal HFSWR and Terrestrial AIS.

5.3.1. *Real Data information.* The SAR image is acquired from RADARSAT2 on 06:52, 13 November 2013, which is wide mode, Vertical Transmit and Vertical Receive (VV) polarisation, with 25*25 m spatial resolution and 10 m pixel spacing. Figure 2(a) shows the SAR image. The SAR measurements are detected by the sliding window Constant False Alarm Rate (CFAR) algorithm (Ji et al., 2010). The

https://doi.org/10.1017/S037346331600062X Published online by Cambridge University Press

Table 2. Main parameters of the simulated scenarios.

SAR parameter	Value	HFSWR	Value
$\sigma_{x,y}$	0·67 km	σ_r	0·15 km ~ 0·67 km
σ_l	3 m ~ 10 m	σ_θ	1·5° ~ 1·67°
σ_w	3 m ~ 10 m	σ_{v_r}	0·36 km/h ~ 0·67 km/h
σ_h	2·5° ~ 5°	P_{Dh}	35%
P_{Ds}	95%	P_{Fh}	10%
P_{Fs}	10%		

Table 3. The association results of different features in the Multi-feature association algorithm.

SAR features	HFSWR features	Accuracy rate	Num_associate
(x, y)	r, θ	63·68%	173
(x, y), length	r, θ	66·12%	178
(x, y), length, width	r, θ	64·26%	174
(x, y), length, width, heading	r, θ	64·03%	172
(x, y)	r, v_r	65·76%	174
(x, y), length	r, v_r	76·08%	197
(x, y), length, width	r, v_r	67·23%	176
(x, y), length, width, heading	r, v_r	66·89%	174
(x, y)	r, θ, v_r	65·10%	170
(x, y), length	r, θ, v_r	66·96%	179
(x, y), length, width	r, θ, v_r	65·64%	172
(x, y), length, width, heading	r, θ, v_r	65·31%	170

Table 4. The comparison of three association algorithms.

	NN association	Position ML association	Multi-feature ML association
Mean Position error (km)	0·97	0·98	1·00
Mean Range error (km)	0·81	0·77	0·75
Mean Azimuth error (°)	1·48	1·37	1·55
Mean Radial Velocity error (km/h)	0·81	0·80	0·72
accuracy rate	60·23%	63·68%	76·08%
num_right	155	173	197

ship length is extracted by the rotation and pixel counting method (Margarit and Tabasco, 2011).

The HFSWR data is collected from coastal HFSWR, whose working frequency is 4·70 MHz. The number of antenna array elements is eight, and the distance of antenna elements is 14·5 m. The time span of data collected is 1 min. The HFSWR measurements are detected with the CFAR method of Adaptive Power Regression Thresholding (APRT) (Dzvonkovskaya and Hermann, 2007).

The AIS data are collected from Terrestrial AIS. Since the AIS report time relies on the type of AIS equipment and ship dynamic state, the time span of AIS report is from 06:47 to 06:57 on 13 November 2013. The DR method is used to deduce the ship dynamic state at the satellite transit time using the AIS report.

https://doi.org/10.1017/S037346331600062X Published online by Cambridge University Press

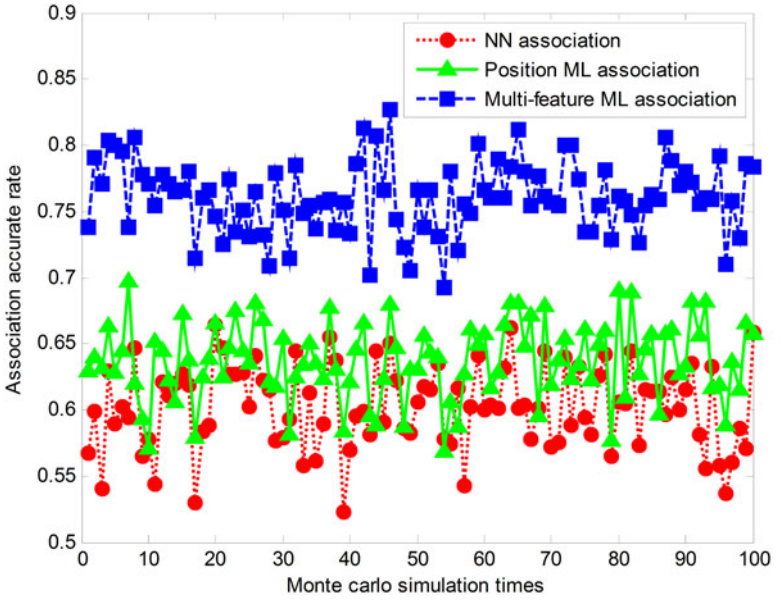

Figure 1. Association results of NN, position ML and Multi-feature ML association.

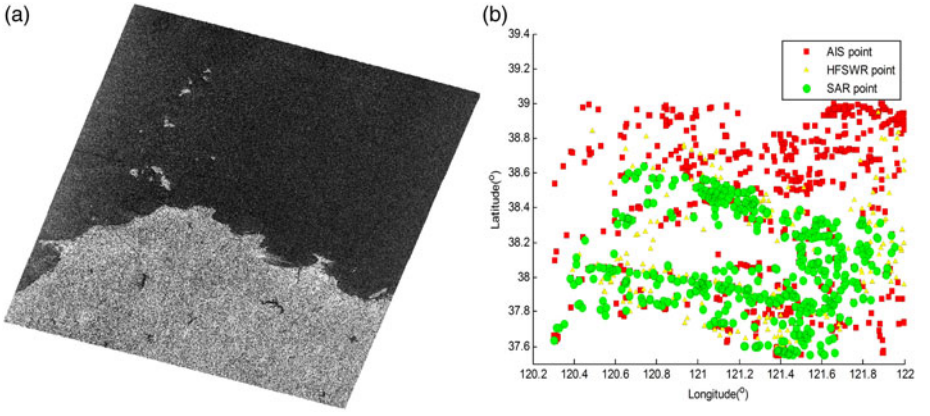

Figure 2. The SAR image and SAR, HFSWR, AIS measurements on 13 November 2013.

Figure 2(b) presents the distribution of three sensors measurements, which covers the range of Northern latitude 37·5° ~ 39° and East longitude 120·2° ~122°. The square points represent the AIS measurements; the triangular points represent the HFSWR measurements; the circular points represent the SAR measurements. The number of AIS, HFSWR and SAR measurements is 672, 212, and 478, respectively.

5.3.2. *Real Data association result.* Table 5 shows the association results. The number of cooperative ships detected by at least two sensors is 299. This is because

https://doi.org/10.1017/S037346331600062X Published online by Cambridge University Press

Table 5. The association results of the real ship detection scenario.

Detected sensor	Cooperative ships				Non-cooperative ships
	SAR&HFSWR&AIS	SAR&AIS	HFSWR&AIS	AIS	SAR&HFSWR
The number of association results	53	240	6	373	58

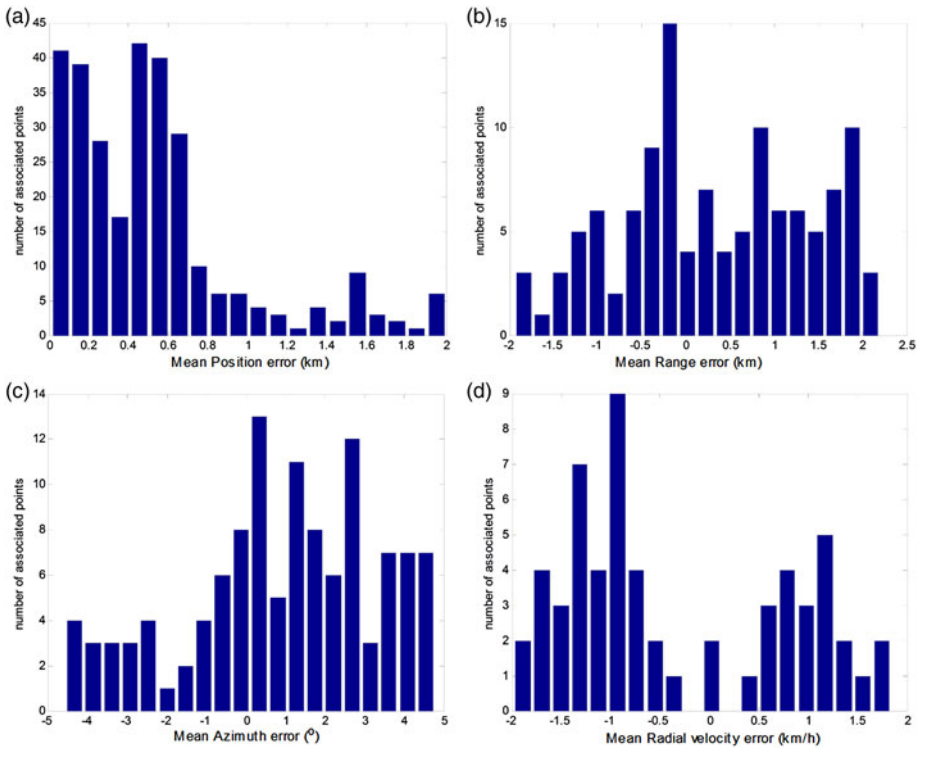

Figure 3. The distribution of Mean position, range azimuth and radial velocity error.

the AIS coverage area is wider than the SAR and HFSWR, and the rest of the 373 cooperative ships are only detected by AIS. The number of non-cooperative ships is 58.

The association error is also analysed. Figure 3 illustrates the distribution of the different errors. The position errors are in the range $0 \sim 2$ km, and mean position error is about 0·53 km. The signed range errors are in the range of $-2 \sim 2$ km, and the mean range error is about 0·93 km. The signed azimuth errors are distributed between -5 and 5°, and mean azimuth error is 2·13°. The signed Radial Velocity Errors lie between $-2 \sim 2$ km/h, and mean radial velocity error is about 1·08 km/h.

A local area data is also employed to demonstrate the effect of different association algorithms. Figure 4 shows the local area, the range of Northern latitude 37·91° ~ 37·97° and East longitude 121·09° ~121·15°. There are five AIS measurements, four HFSWR measurements and six SAR measurements, which are labelled by the

https://doi.org/10.1017/S037346331600062X Published online by Cambridge University Press

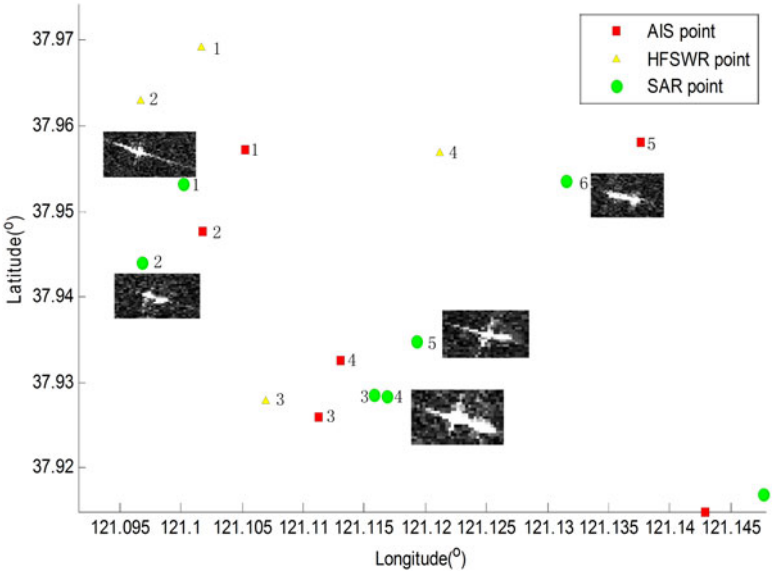

Figure 4. The local area of Figure 2.

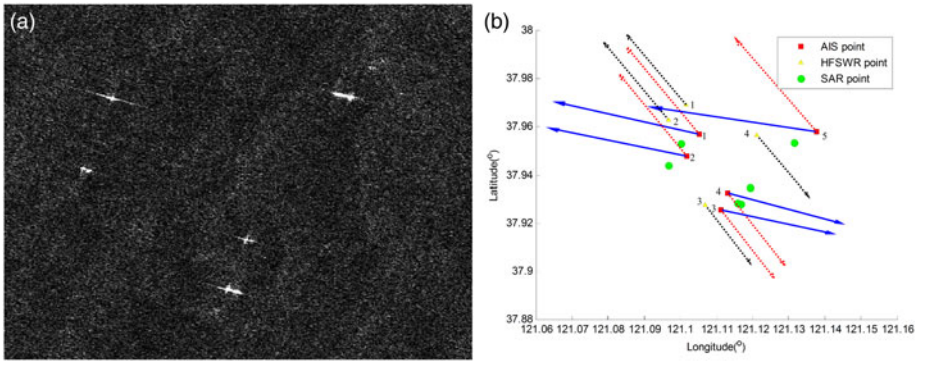

Figure 5. Ships in the SAR image and the radial velocity diagram.

symbols and number. Figure 5(a) is the corresponding SAR image of the local area, in which only five ships are clearly identified. The SAR measurement 3 in Figure 4 possibly originates from a false alarm, and the other five ship images are all labelled in Figure 4. Figure 5 (b) highlights the radial velocity direction of the AIS and HFSWR measurements. The arrow of the solid line represents the course over ground of AIS measurements, and the arrow of the dotted line represents the direction of radial velocity. Table 6 shows the speed of the AIS and HFSWR measurements.

Table 7 shows the association results of three algorithms. The results set $\{i_a, i_h, i_s\}$ means that the i_ath AIS measurement, the i_hth HFSWR measurement and the i_sth SAR measurement all originate from the same target. $i = 0$ means that the target is missed by this sensor. The NN and position ML algorithms made a mistake in the

https://doi.org/10.1017/S037346331600062X Published online by Cambridge University Press

Table 6. The speed of AIS and HFSWR measurements.

AIS				HFSWR	
Number	v_{sog}(knot)	θ_{cog}(°)	v_r(km/h)	Number	v_r(km/h)
1	11·3	288	−20·58	1	−21·11
2	10·7	287	−19·43	2	−19·27
3	9·2	111	16·93	3	16·22
4	8·8	107	16·07	4	16·76
5	12·6	282	−22·24		

Table 7. The association results of three algorithms.

algorithm	Association results $\{i_a, i_h, i_s\}$
NN Association	{1,1,1} {2,2,2} {3,3,3} {4,4,0} {5,0,6} {0,0,5}
Position ML association	{1,1,1} {2,2,2} {3,3,3} {4,4,4} {5,0,6} {0,0,5}
Multi-feature ML association	{1,1,1} {2,2,2} {3,3,4} {4,4,5} {5,0,6}

association because of the presence of the SAR measurement 3. Multi-feature ML association results are more reasonable.

Details of multi-feature ML association results are analysed as follows. The results {1, 1, 1} and {2, 2, 2} originate from two cooperative ships, which are detected by all three sensors. From the fusion information, it is derived that the ship of {1, 1, 1} is an oil tanker, whose length is 93 m, the other ship of {2, 2, 2} is a cargo vessel, whose length is 98 m. The result {5, 0, 6} is a cooperative ship detected by the SAR and AIS, which is mis-detected by the HFSWR. The direction of HFSWR measurement 4 radial velocity is inconsistent with direction of the AIS measurement 5 radial velocity. Therefore, The HFSWR point 4 does not originate from the target {5, 0, 6}. The merit of multi-feature ML association is demonstrated in the association of the measurements {3, 3, 4} and {4, 4, 5}. When we considered the multi-feature (ship length and radial velocity) in the association, the wrong association, caused by the SAR measurement 3, can be avoided. We deduced that the target {3, 3, 4} is a cooperative cargo and the target {4, 4, 5} is a cooperative oil tanker.

6. CONCLUSIONS. Data fusion of Space-borne SAR, HFSWR and AIS for ship detection can improve the detection accuracy and reduce false alarms. Data association is the key step in data fusion. In order to make full use of the measurements, a multi-feature ML association algorithm is proposed in this paper. Besides the traditional position information, we employed the ship length, width, heading and radial velocity data in the data association. Results from simulated data demonstrated that ship width and heading for SAR, and azimuth for the HFSW did not improve the results of the association of medium resolution SAR and low resolution HFSWR. Real data results showed that the multi-feature ML association algorithm can improve the association accuracy under the condition of measurements with some false alarms. From the association results, we can further identify the information of cooperative ships and suspected non-cooperative ships. The non-cooperative ships are regarded as the track start point for the non-cooperative ship tracking. Since the medium

https://doi.org/10.1017/S037346331600062X Published online by Cambridge University Press

resolution Space-borne SAR measurements cannot provide accurate target velocity, the association of SAR and HFSWR measurements can only depend on the position data, which reduced the association accuracy. Future work will be concentrated on obtaining more high resolution information from SAR and HFSWR.

FINANCIAL SUPPORT

This work was supported by the National Natural Science Foundation of China (Grant number 61362002), Marine scientific research special funds for public welfare (Grant No. 201505002), and the Postgraduate Scientific Research Innovation Key Foundation of Inner Mongolia (Grant number 1402020201).

REFERENCES

Brusch, S., Lehner, S., Fritz, T., Soccorsi, M., Soloviev, A. and Van Schie, B. (2011). Ship Surveillance With TerraSAR-X. *IEEE Transactions on Geoscience and Remote Sensing*, **49**, 1092–1103.

Chaturvedi, S.K., Yang, C.S., Ouchi, K. and Shanmugam, P. (2012). Ship Recognition by Integration of SAR and AIS. *Journal of Navigation*, **65**, 323–337.

Deb, S., Yeddanapudi, M., Pattipati, K. and Bar-Shalom, Y. (1997). A generalized S-D assignment algorithm for multisensor-multitarget state estimation. *IEEE Transactions on Aerospace and Electronic Systems*, **33**, 523–538.

Dzvonkovskaya, A. and Rohling, H. (2010). HF radar performance analysis based on AIS ship information. *Proceedings of 2010 IEEE Radar Conference*, Virginia, USA.

Dzvonkovskaya, A., and Hermann, R. (2007). Ship Detection with Adaptive Power Regression Thresholding for HF Radar. *Radar Science and Technology*, **2**, 81–85.

Dzvonkovskaya, A., Gurgel, K.W., Rohling, H. and Schlick, T. (2008). Low power High Frequency Surface Wave Radar application for ship detection and tracking. *Proceedings of 2008 International Conference on radar*, Adelaide, Australia.

Fingas, M.F. and Brown, C.E. (2001). Review of ship detection from airborne platforms. *Canadian Journal of Remote Sensing*, **27**, 379–385.

Grosdidier, S., Baussard, A. and Khenchaf, A. (2010). HFSW radar model: Simulation and measurement. *IEEE Transactions on Geoscience and Remote Sensing*, **48**, 3539–3549.

Gurgel, K.W., Schlick, T., Horstmann, J. and Maresca, S. (2010). Evaluation of an HF-radar ship detection and tracking algorithm by comparison to AIS and SAR data. *Proceedings of 2010 International Waterside Security Conference (WSS)*, Carrara, Italy.

Habtemariam, B., Tharmarasa, R., Mcdonald, M. and Kirubarajan, T. (2015). Measurement level AIS/radar fusion. *Signal Processing*, **106**, 348–357.

Hall, D. and Llinas, J. (1997). An introduction to multisensor data fusion. *Proceedings of the IEEE*, **85**, 6–23.

Ji, Y., Zhang, J., Meng, J. and Wang, Y. (2014). Point association analysis of vessel target detection with SAR, HFSWR and AIS. *Acta Oceanologica Sinica*, **33**, 73–81.

Ji, Y., Zhang, J., Meng, J. and Zhang, X. (2010). A new CFAR ship target detection method in SAR imagery. *Acta Oceanologica Sinica*, **29**, 12–16.

Jonker, R. and Volgenant, A. (1987). A shortest augmenting path algorithm for dense and sparse linear assignment problems. *Computing*, **38**, 325–340.

Kadar, I., Eadan, E.R. and Gassner, R.R. (1997). Comparison of robustized assignment algorithms. *Proceedings of* 1997 *International Society for Optics and Photonics AeroSense'97*. Orlando, USA.

Li, X.R. and Jilkov, V.P. (2003). Survey of maneuvering target tracking. Part I. Dynamic models. *IEEE Transactions on Aerospace and Electronic Systems*, **39**, 1333–1364.

Malkoff, D.B. (1997). Evaluation of the Jonker-Volgenant-Castanon (JVC) assignment algorithm for track association. *Proceedings of* 1997 *International Society for Optics and Photonics AeroSense'97*. Orlando, USA.

Maresca, S., Braca, P., Horstmann, J. and Grasso, R. (2014). Maritime surveillance using multiple high-frequency surface-wave radars. *IEEE Transactions on Geoscience and Remote Sensing*, **52**, 5056–5071.

Margarit, G. and Tabasco, A. (2011). Ship Classification in Single-Pol SAR Images Based on Fuzzy Logic. *IEEE Transactions on Geoscience and Remote Sensing*, **49**, 3129–3138.

Pattipati, K.R., Deb, S., Bar-Shalom, Y. and Washburn, R.B. (1992). A new relaxation algorithm and passive sensor data association. *IEEE Transactions on Automatic Control*, **37**, 198–213.

Pichel, W., Clemente-Colon, P., Wackerman, C. and Friedman, K. (2004). Ship and wake detection. *Synthetic aperture radar marine user's manual, US Department of Commerce, National Oceanic and Atmospheric Administration, National Environmental Satellite, Data, and Information Serve, Office of Research and Applications*, 277–303.

Ponsford, A.M. and Wang, J. (2010). A review of high frequency surface wave radar for detection and tracking of ships. Special Issue on ky-and Ground-wave High Frequency (HF) Radars: Challenges in Modelling, Simulation and Application, Turkish Journal of Electrical Engineering and Computer Sciences, **18**, 409–428.

Poore, A.B. and Robertson, A.J., III (1997). A new Lagrangian relaxation based algorithm for a class of multidimensional assignment problems. *Computational Optimization and Applications*, **8**, 129–150.

Tunaley, J.K. (2003). The estimation of ship velocity from SAR imagery. *Proceedings of 2003 International Geoscience and Remote Sensing Symposium*. Toulouse, France.

Vivone, G., Braca, P. and Horstmann, J. (2015). Knowledge-Based Multitarget Ship Tracking for HF Surface Wave Radar Systems. *IEEE Transactions on Geoscience and Remote Sensing*, **53**, 3931–3949.

Xiao, F., Ligteringen, H., Van Gulijk, C. and Ale, B. (2015). Comparison study on AIS data of ship traffic behavior. *Ocean Engineering*, **95**, 84–93.

Zhang, H., Liu, Y.X., Zhang, J., Ji, Y.G. and Zheng, Z.Q. (2015). Target point tracks optimal association algorithm with surface wave radar and automatic identification system. *Dianzi Yu Xinxi Xuebao/ Journal of Electronics and Information Technology*, **37**, 619–624.

Zhao, Z., Ji, K., Xing, X., Zou, H. and Zhou, S. (2014a). Ship Surveillance by Integration of Space-borne SAR and AIS-Review of Current Research. *Journal of Navigation*, **67**, 177–189.

Zhao, Z., Ji, K., Xing, X., Zou, H. and Zhou, S. (2014b). Ship Surveillance by Integration of Space-borne SAR and AIS - Further Research. *Journal of Navigation*, **67**, 295–309.